Ultrafast Relaxation of Excited Dirac Fermions in Epitaxial Graphene Using Optical Differential Transmission Spectroscopy

Dong Sun,[1] Zong-Kwei Wu,[1] Charles Divin,[1] Xuebin Li,[2] Claire Berger,[2] Walt A. de Heer,[2] Phillip N. First,[2] and Theodore B. Norris[1,*]

[1]*Center for Ultrafast Optical Science, University of Michigan, Ann Arbor, Michigan 48109-2099, USA*
[2]*School of Physics, Georgia Institute of Technology, Atlanta, Georgia 30332, USA*

(Received 15 March 2008; published 6 October 2008)

We investigate the ultrafast relaxation dynamics of hot Dirac fermionic quasiparticles in multilayer epitaxial graphene using ultrafast optical differential transmission spectroscopy. We observe differential transmission spectra which are well described by interband transitions with no electron-hole interaction. Following the initial thermalization and emission of high-energy phonons, the electron cooling is determined by electron-acoustic phonon scattering, found to occur on the time scale of 1 ps for highly doped layers, and 4–11 ps in undoped layers. The spectra also provide strong evidence for the multilayer structure and doping profile of thermally grown epitaxial graphene on SiC.

DOI: 10.1103/PhysRevLett.101.157402 PACS numbers: 78.47.−p, 78.40.Ri, 78.66.Tr

Graphene is a planar layer of carbon atoms in a hexagonal lattice, with a linear energy spectrum near the intersection of the electron and hole cones in the band structure (the Dirac point) [1–4]. The linear energy dispersion gives rise to massless Dirac quasiparticles with an energy-independent velocity, leading to unusual quantum properties [5–9] and an electrodynamic response differing significantly from that of fermionic plasmas with parabolic dispersion [10,11]. Graphene grown expitaxially on SiC substrates has been proposed as a platform for carbon-based nanoelectronics [12,13]. Both transport measurements and infrared spectroscopy have provided strong evidence that the band structure of epitaxial graphene layers is essentially the same as for single-layer graphene [14–19]. While transport in steady-state measurements is controlled by the electrons near the Fermi level, transport in high speed devices is determined by the dynamic conductivity of hot carriers, i.e., electrons whose temperature is elevated above the lattice temperature due to the presence of high fields and/or dynamic fields in the material. It is critical therefore to understand both the cooling of the electrons due to coupling to lattice phonons and the response of the quasiparticle plasma to dynamical fields.

Here we report the first ultrafast spectroscopy of hot Dirac quasiparticles in epitaxial graphene in the region near the Fermi level [20]. As illustrated in Fig. 1, a 100-fs near-infrared (800 nm) optical pulse excites quasiparticles from the valence to the conduction band across the Dirac point; the optical response of a multilayer graphene structure containing both doped and undoped layers is measured via the differential transmission (DT) of a tunable probe pulse as a function of pump-probe delay. The electrons have an initial energy of 428 meV above the Fermi level in the doped layers and 777 meV in the undoped layers. Because of rapid carrier-carrier scattering, a hot thermal distribution is established within the time resolution of the experiment (150 fs). This distribution cools towards the lattice temperature, initially via the emission of high-energy (194 and 330 meV) phonons [21], and later via the interaction with acoustic phonons. In these experiments, the elevated temperature of the quasiparticles is manifested primarily through the modification of the probe absorption by Pauli blocking of interband transitions.

For the optical experiments, a 100-fs 250-kHz amplified Ti:sapphire laser at 800 nm pumps an infrared optical parametric amplifier with signal wavelength tunable from 1.1 to 1.6 μm and idler tunable from 1.6–2.6 μm. The sample is pumped with pulses at 800 nm, and either the signal or the idler is used as the probe; the temporal resolution is 150 fs, determined through both cross-correlation measurements and the DT rise time. The

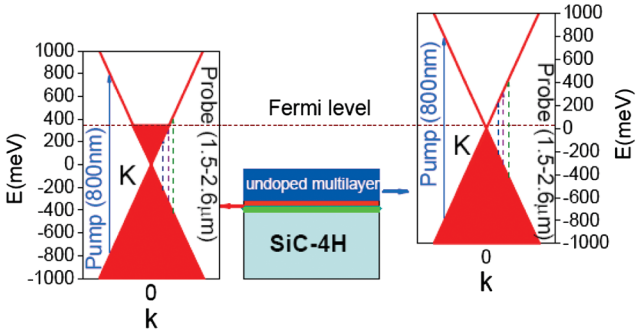

FIG. 1 (color). Sample structure and energy dispersion curves of doped and undoped graphene layers. The sample has a buffer layer (green) on the SiC substrate followed by 1 heavily doped layer (red) and approximately 20 undoped layers (blue) on top. The Fermi level is labeled with a dashed line (brown) lying 348 meV (from the later data) above the Dirac point of the doped graphene layer and passing through the Dirac point of the undoped graphene layers. The blue solid line shows the transitions induced by the 800-nm optical pump pulse; the three dashed lines correspond to probe transitions at different energies with respect to the Fermi level (discussed in the text).

pump and probe beams are colinearly polarized and focused on the sample to 80- and 40-μm diameter spots, respectively. The probe beam after the sample is filtered in a monochromator with 3-nm resolution and detected by an InGaAs photodetector and lock-in amplifier referenced to the 4.2-kHz mechanically chopped pump. The sample temperature is controlled over a range 10–300 K.

The sample is an ultrathin epitaxial graphene film produced on the C-terminated $(000\bar{1})$ face of single-crystal 4H-SiC by thermal desorption of Si [16,17]. Figure 1 shows the structure of the sample [13,14,17,22]: the first carbon layer (green) is covalently bonded to the 4H-SiC substrate and acts as a buffer layer; the following layer (red) exhibits the graphene electronic spectrum and is doped by charges transferred from the SiC. From the measured Fermi level (see below), the charge density is estimated to be 9×10^{12} electrons/cm^2. The graphene layers (blue) above the doped layer are neutral [22,23]. For the growth conditions employed, the number of neutral layers has been estimated to be in the range 15–20 [15,24].

Figure 2(a) shows representative DT spectra at various probe time delays. The DT amplitude peaks near zero time delay for all probe wavelengths; since the DT rise time is limited by the experimental time resolution, a hot thermal carrier distribution is apparently established on a time scale much less than 150 fs. The DT amplitude then relaxes towards zero on a time scale of 15 ps. The DT signal flips from positive on the blue (high-energy) side of a probe wavelength of 1.78 μm to negative on the red (low-energy) side of 1.78 μm, and flips back from negative to positive again at 2.35 μm.

Figures 2(b) and 2(c) show DT time scans for selected probe wavelengths on both red and blue sides of the two zero crossings. Immediately following the pump pulse, the DT signal is positive over the entire probe spectral range. The DT signal becomes negative within 2 ps if the probe wavelength falls between 1.78 and 2.35 μm, otherwise it remains positive until the signal decays away. The DT signal relaxes to zero on the time scale of 1–10 ps depending on probe wavelength. The lack of the data in the two blank regions of Fig. 2(a) is due to limitations in tuning our optical parametric amplifier.

Figure 3 shows the effect of lattice temperature on the carrier dynamics (the data are taken at a different position from that in Fig. 2). For spectral regions where the DT sign is positive, the DT dynamics show little temperature dependence apart from minor amplitude changes and slightly

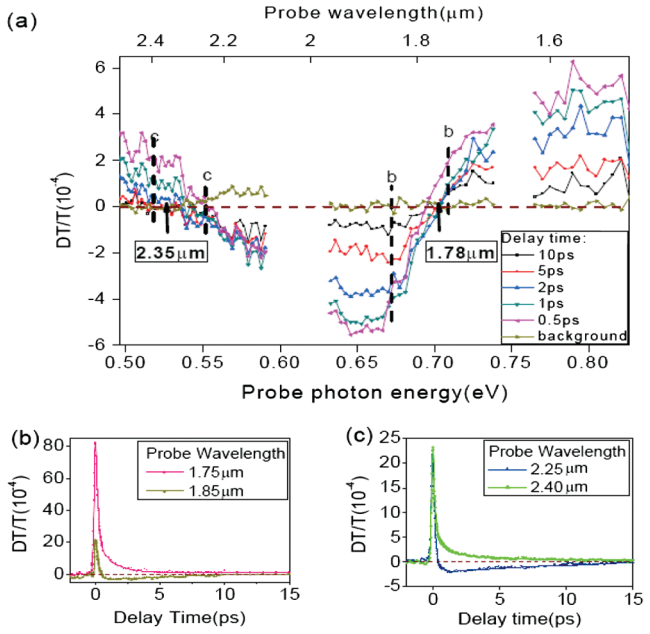

FIG. 2 (color). DT spectrum normalized by transmission (T). (a) DT spectrum on epitaxial graphene at 10 K, with 500-μW 800-nm pump (photon fluence of 1.6×10^{14} photons/cm^2 per pulse), at probe delays of 10, 5, 2, 1, 0.5 ps, and background (50 ps before the pump arrives). The arrows at 1.78 and 2.35 μm indicate the DT zero crossings. (b) DT time scan of the two probe wavelengths marked in (a) at the red (1.85 μm) and blue side (1.75 μm) of the 1.78 μm DT zero crossing. (c) Time scan of the two probe wavelengths marked in (a) at the red (2.40 μm) and blue side (2.25 μm) of the 2.35 μm DT zero crossing. In all figures, the dashed line (brown) marks where the DT signal is zero. The DT tails in (b) and (c) are simply fitted by a sigmoidal curve.

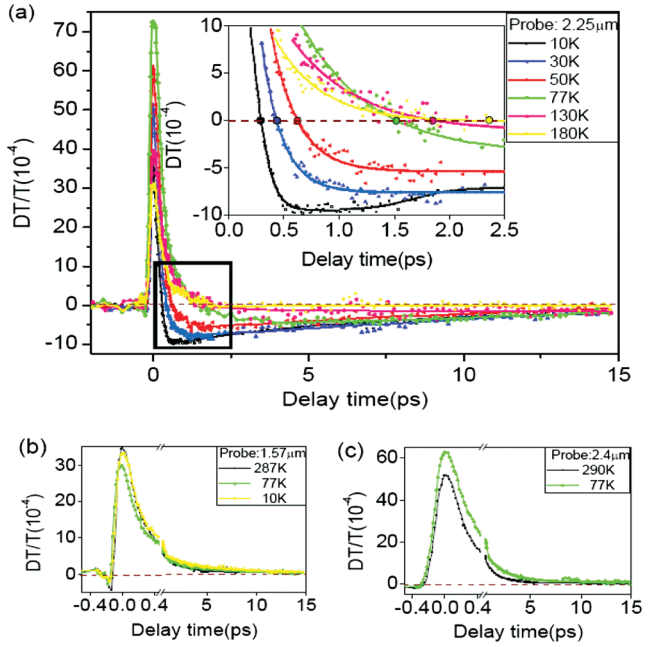

FIG. 3 (color). Temperature dependent DT spectrum. (a) DT time scans at temperature 10, 30, 50, 77, 130, and 180 K with 500 μW pump at 800 nm and 2.25 μm probe. The DT time scans were fit with a sigmoidal curve to show more clearly the behavior of the zero crossings. In the inset the DT zero-crossing points at different temperatures are marked with different colors. (b) DT time scans at temperatures of 10, 77, and 287 K with 1 mW pump at 800 nm and 1.57 μm probe. (c) DT time scans at temperatures of 77 and 290 K with 1 mW, 800 nm pump and 2.4 μm probe. In all figures, the dashed line (brown) marks where the DT is zero.

different relaxation times. When the probe wavelength falls between 1.78 and 2.35 μm, the DT signal is positive at early times, and becomes negative within a few picoseconds. The amplitude of the negative DT component decreases with increasing temperature and almost disappears for temperatures above 180 K. The delay time at which the DT crosses zero increases monotonically with temperature [Fig. 3(a) inset).

We now turn to the interpretation of the DT and the origin of the zero crossings. From the simplest point of view, the differential probe transmission spectrum arises from the change in carrier occupation functions in the bands, since generally the probe absorption is proportional to $f_v(1 - f_c)$ where f_v (f_c) is the occupation probability in the valence (conduction) band. Following the excitation of quasiparticles high into the conduction band by the pump, electron-electron scattering on a time scale short compared to 150 fs establishes a hot thermal distribution. Since the carrier occupation probability above the Fermi energy is increased by the pump, the DT signal is positive due to reduced probe absorption. Below the Fermi level, the heating of the electron plasma reduces the occupation probability, so the DT is negative. Thus the upper zero crossing at 1.78 μm probe wavelength arises from the smearing of the Fermi level in the doped layers. We find the Fermi level μ_d for the doped layer to be 348 meV above the Dirac point. This result is close to the calculated Fermi level in the carbon-deficient geometry [22], and is consistent with the results of transport studies on epitaxial graphene grown on the C-terminated $(000\bar{1})$ face [13]. We note additionally that there is no peak in the DT spectrum near the Fermi level; this indicates that there is no Fermi edge singularity [25,26] due to electron-hole interactions in the interband absorption spectrum of graphene, as may be expected from the massless nature of the quasiparticles.

At very long probe wavelengths, i.e., for transition final states well below the Fermi level of the doped layers, one may expect the DT spectra to be determined primarily by the carrier occupations in the undoped layers; since the pump pulse generates hot carriers in the undoped layers, the sign of the DT signal arising from the undoped layers should be positive for all wavelengths. However, for probe wavelengths below the Fermi level of the doped layer, the contribution of the doped layer to the DT is negative. Thus one expects that for some probe energy the net DT signal should flip sign; this is the origin of the lower zero crossing at 2.35 μm.

The probe transmission and reflection spectra were self-consistently modeled using the transfer-matrix method, incorporating both the interband and intraband contributions to the dynamic conductivity (or dielectric constant) of each graphene layer [4,11]. We calculated the transmission spectrum of the multilayer structure of Fig. 1, with transfer matrices for 20 undoped graphene layers (Fermi level at the Dirac point) and 1 doped layer [25] with a Fermi level of 350 meV.

Figure 4 shows the calculated transmission spectrum for various electron temperatures, where for simplicity we have assumed the temperature to be the same for all layers. At low temperature (10 K), the transmission spectrum shows an absorption edge at $\hbar\omega = 2\mu_d$, as one would expect from the simple picture of interband absorption discussed previously. Here μ_d is the Fermi level energy relative to the Dirac point of the doped layer. As the temperature increases, the absorption edge due to the doped layer broadens due to smearing of the carrier distribution around the Fermi level, and the undoped layers contribute a broad peak at low energy.

Figure 4(b) shows the calculated DT spectrum for an initial electron temperature of 10 K (i.e., the DT spectrum is the transmission spectrum for an elevated electron temperature minus the transmission spectrum for 10 K). The DT spectra show the upper and lower zero crossings at energies ($\hbar\omega = 2\mu_d$ and $\hbar\omega \approx 1.5\mu_d$, respectively) close to those observed in the experiment. The calculated DT signal is positive over the entire spectral range if the electron temperature is higher than approximately 960 K; since the experimental DT immediately following the pump pulse is positive everywhere, this establishes that the initial carrier temperature exceeds 960 K.

Examination of Fig. 4 shows that when the probe energy is between the two DT zero crossings, the transmission curve does not relax monotonically with decreasing elec-

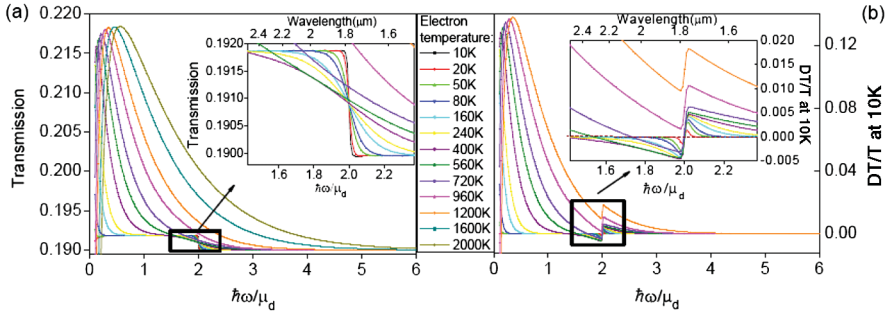

FIG. 4 (color). DT signal simulation. (a) Simulated transmission curves at different electron temperatures. In the inset, the transmission curves at low electron temperature are shown expanded for frequencies around the two DT zero crossings. (b) Simulated DT/T curves at different electron temperatures with lattice temperature at 10 K. In the inset, the DT/T curves for low electron temperatures are expanded in the vicinity of the two DT zero crossings. Both figures share the same legend.

tron temperature; it decreases to a minimum around 400 K and then turns back and increases with decreasing temperature. The high initial electron temperature gives a positive DT signal; as the carriers lose energy, the DT amplitude decreases and becomes zero for an electron temperature of approximately 700 K. The DT is then negative and reaches its maximum negative amplitude for an electron temperature of 400 K. With further cooling, the DT approaches zero. The time delay at which the DT flips sign should increase with lattice temperature from the model, as observed in the experiment [inset of Fig. 3(a)].

In contrast, when the probe wavelength is either above the upper or below the lower zero crossing, the transmission decreases monotonically with the electron temperature and the DT decay curves are only weakly dependent on lattice temperature, as is apparent in Figs. 3(b) and 3(c).

Additional simulations performed by excluding various contributions to the total conductivity reveal that the dominant contribution is the real part of the interband conductivity. We note that the observed lower zero crossing is unrelated to the transverse electric mode arising from the negative imaginary part of the interband conductivity predicted in recent work [11]. The imaginary intraband conductivity only results in a small shift of the lower zero crossing (less than 5%), and this contribution cannot be isolated in our normal-incidence DT experiment. Our DT spectra are well described by interband transitions and the single-particle density of states for linear dispersion, and no electron-hole interaction; investigations of the intraband response will require much longer probe wavelengths. We also note that the simulations are sensitive to the detailed layer structure of the epitaxial graphene, and the spectra provide strong corroborating evidence for the epitaxial graphene structure determined using other methods [14–19]; our best fit to the data is obtained for one conducting layer and 20 undoped layers.

Our calculations of the DT assume that the quasiparticle plasma can be described by a thermal distribution characterized by a single electron temperature T_e in all layers. Within the time resolution of our experiment, the electron distribution appears to be thermal in all experimental DT spectra. From the time delay of zero-crossing DT point at 10 K, we find that the hot electron temperature relaxes to around $T_e = 420$ K (36 meV) on the time scale of 1.7 ps by emitting two or three 197 meV [21] optical G phonons [27,28], or one to two 330 meV D phonons [21]. The relaxation afterwards is mainly due to the relatively slow acoustic phonon scattering process. Because the photoinjected carrier population is low (less than 1.2×10^{11} cm^{-2} per layer), the probe DT is sensitive only to the high-energy thermal tail of the carrier distribution at the probe wavelengths used, so the dynamics are interpreted only in terms of carrier cooling, and the experiments are insensitive to possible electron-hole recombination across the Dirac point.

To determine the electron temperature T_e as a function of time from the DT amplitudes, we calculate the DT at a given probe wavelength for each value of the temperature. We find that fits of the DT dynamics near the upper zero crossing (where the DT is dominated by the doped layer) show that the decay of T_e is reasonably well described by a single exponential with a time constant of 1.45 ps. Fits to the DT dynamics near the lower zero crossing cannot be fit with single exponential decay of T_e, but can be well fit by a stretched exponential $\exp[-(t/\tau)^{1/h}]$ with τ in the range of 4–11 ps and a heterogeneity parameter $h = 3$. The long nonexponential decay may arise from the generation of hot phonons [27,28] although disorder in the sample or the temperature- and density-dependence of the scattering rate may also contribute. The observed time scale for the cooling is consistent with the 4-ps electron-phonon scattering time constant estimated recently from magnetoresistance measurements [13] and with recent calculations [27].

This project has been supported by NSF grants ECCS-0404084 and ECCS-0521041.

*Author to whom correspondence should be addressed. tnorris@eecs.umich.edu

[1] K. S. Novoselov *et al.*, Science **306**, 666 (2004).
[2] S. Y. Zhou *et al.*, Nature Phys. **2**, 595 (2006).
[3] P. R. Wallace, Phys. Rev. **71**, 622 (1947).
[4] G. W. Semenoff, Phys. Rev. Lett. **53**, 2449 (1984).
[5] G. M. Rutter *et al.*, Science **317**, 219 (2007).
[6] Y. Zhang *et al.*, Nature (London) **438**, 201 (2005).
[7] K. S. Novoselov *et al.*, Nature (London) **438**, 197 (2005).
[8] E. McCann *et al.*, Phys. Rev. Lett. **97**, 146805 (2006).
[9] X. Wu *et al.*, Phys. Rev. Lett. **98**, 136801 (2007).
[10] V. P. Gusynin, S. G. Sharapov, and J. P. Carbotte, Phys. Rev. Lett. **96**, 256802 (2006).
[11] S. A. Mikhailov and K. Ziegler, Phys. Rev. Lett. **99**, 016803 (2007).
[12] C. Berger *et al.*, J. Phys. Chem. B **108**, 19 912 (2004).
[13] C. Berger *et al.*, Science **312**, 1191 (2006).
[14] M. L. Sadowski *et al.*, Solid State Commun. **143**, 123 (2007).
[15] J. Hass *et al.*, Phys. Rev. B **75**, 214109 (2007).
[16] P. Darancet, N. Wipf, and D. Mayou, arXiv:0711.0940.
[17] W. A. de Heer *et al.*, Solid State Commun. **143**, 92 (2007).
[18] M. L. Sadowski *et al.*, Phys. Rev. Lett. **97**, 266405 (2006).
[19] J. Hass *et al.*, Phys. Rev. Lett. **100**, 125504 (2008).
[20] J. M. Dawlaty *et al.*, Appl. Phys. Lett. **92**, 042116 (2008).
[21] C. Faugeras *et al.*, Appl. Phys. Lett. **92**, 011914 (2008).
[22] F. Varchon *et al.*, Phys. Rev. Lett. **99**, 126805 (2007).
[23] A. Mattausch and O. Pankratov, Phys. Rev. Lett. **99**, 076802 (2007).
[24] J. Hass *et al.*, Appl. Phys. Lett. **89**, 143106 (2006).
[25] H. Kalt *et al.*, Phys. Rev. B **40**, 12 017 (1989).
[26] T. Uenoyama and L. J. Sham, Phys. Rev. Lett. **65**, 1048 (1990).
[27] S. Butscher *et al.*, Appl. Phys. Lett. **91**, 203103 (2007).
[28] T. Kampfrath *et al.*, Phys. Rev. Lett. **95**, 187403 (2005).